Available online at www.eccomasproceedia.org
Eccomas Proceedia COMPDYN (2023) 2946-2962

ECCOMAS
Proceedia

COMPDYN 2023
9th ECCOMAS Thematic Conference on
Computational Methods in Structural Dynamics and Earthquake Engineering
M. Papadrakakis, M. Fragiadakis (eds.)
Athens, Greece, 12-14 June 2023

ASSESSMENT OF MACRO-ELEMENTS IN THE PREDICTION OF THE RESPONSE OF OFFSHORE WIND TURBINES

Olgu Orakci[1], Nunzia Letizia[1], Stijn François[2], Shiaohuey Chow[3], Yinghui Tian[3], George Anoyatis[1*]

[1] KU Leuven, Department of Civil Engineering, Hydraulics and Geotechnics Section
Bruges, Belgium

[2] KU Leuven, Department of Civil Engineering, Structural Mechanics Section
Leuven, Belgium

[3] University of Melbourne, Department of Infrastructure Engineering, Offshore Geomechanics Group
Melbourne, Australia

[*]corresponding author, e-mail: @george.anoyatis@kuleuven.be

Abstract. *The dynamic excitation of Offshore Wind Turbines (OWTs) by wind, waves, and currents is an important issue to harness offshore wind energy, where the estimation of the OWT natural frequency is a key aspect. Advanced numerical models and simplified methodologies are used in engineering practice to optimize the design and performance of the turbines. This work provides an assessment of existing tools to determine the natural frequency and response of OWTs, by presenting an engineering study of an OWT in the general Dunkirk sand model from the PISA project. The selected foundation type is a hollow steel monopile, which is typically used in shallow-to-mid water depths and is a cost-effective solution to support the dead weight of the turbine and the environmental loads it experiences during the life span. In particular, this study involves: (i) the interpretation of geotechnical data from the PISA project Dunkirk site; (ii) the design of the monopile using spring models from PISA methodology for lateral springs, and the recently published unified method for vertical springs along the monopile shaft and at the base and following the API and DNV guidelines. This includes results from modeling the monopile as a Timoshenko beam; (iii) the selection of appropriate macro-elements from the literature to describe the relationship between load and displacement, and thus provide the pile head stiffness in swaying, rocking, cross swaying-rocking; (iv) the implementation of the selected macro-elements to predict the natural frequency of the system and its response using an available method by Arany et al. (2016) and the open source software OpenSees, respectively; (v) the assessment of the adopted simplified methodology for the study selected, using comparisons with results obtained from a finite element model.*

Keywords: Offshore wind turbines, Simplified method, Design of monopile, Dynamic analysis

ISSN:2623-3347 Published by Eccomas Proceedia.
Peer-review under responsibility of the organizing committee of COMPDYN 2023.
doi: 10.7712/120123.10613.21454

1 INTRODUCTION

Offshore wind energy is becoming increasingly important as a source of renewable energy. It is a clean and renewable source of electricity that does not produce greenhouse gas emissions or other pollutants which are causing air pollution and climate change. This makes it an attractive alternative to fossil fuels and helps reduce dependence on non-renewable energy sources [2]. It can further increase energy security by diversifying the energy mix and reducing dependence on imported fuels. This can help to stabilize energy prices and reduce exposure to supply disruptions. In light of the above, many countries have set ambitious targets to increase the share of renewable energy in their electricity mix, in order to reduce greenhouse gas emissions and combat climate change. Offshore wind energy is seen as a key technology to help meet these targets, as it has the potential to provide large amounts of clean electricity. The year 2021 witnessed an exceptional increase in new offshore wind capacity installation globally, with a remarkable record of 21 GW, more than three times the capacity deployed in 2020 [11]. New ambitious aims worldwide give promises to new records to come. In particular, the European Union has set a target of installing at least 60 GW of offshore wind capacity by 2030, and 300 GW by 2050, which represents a significant increase from current levels [2]. Offshore wind farms are thus expected to play an increasingly important role in the overall energy system, as they are integrated with other sources of energy, such as onshore wind, solar, and storage, and are connected to the grid, to ensure the stability and reliability of the energy system.

The monopile foundation is a common type of fixed foundation used in offshore wind turbines (OWTs), which consists of a single steel pile driven into the seabed [25]. The foundation is designed to safely resist the loads imposed by wind, waves, and currents. The foundation design is a critical factor in ensuring the safe and reliable operation of OWT foundations, and the consideration of displacements and rotations is an important part of that process, as they affect the OWT performance [22]. Large displacements and rotations can result in fatigue damage to the foundation, tower, and turbine components and serviceability problems which can cause structural failure and operational problems [7].

The stability of an offshore wind turbine depends on limiting displacements and rotations of the foundation within specified thresholds. Specific limits for displacements and rotations are typically imposed by the manufacturer and can vary depending on the specific project conditions [5]. These limits ensure the turbine remains stable and operates efficiently without excessive deformations or structural damage. The response is dependent on the geometrical and mechanical foundation properties, soil conditions, and the loading that the OWT is exposed to in its lifetime [20]. Although an analysis is required by the design guidelines, there is not a unified methodology with a consensus on the serviceability analysis [5].

There are three main categories that can be used to calculate displacements and rotations of monopile foundations: spring methods such as p-y method, advanced methods such as finite element models, and simplified methods such as macro-elements [7]. This work focuses on assessing the performance of a simplified methodology to predict displacement and rotations of OWTs using macroelements available in the literature to represent the monopile-foundation system. The macroelements simplify the analysis significantly and enable a smooth connection to structural analysis by including the soil-foundation system's response at one single point at the base of the OWT (e.g., [17]). Herein a set of simple linear elastic macroelements are used, following the works of Gazetas (1984) [14], Poulos and Davis (1980) [24], Pender(1993) [23], Shadlou and Bhattacharya (2016) [26]. A monopile, which is embedded in a single layer of the "general Dunkirk sand model" (GDSM) of the PISA project [8], is first designed to support an

8 MW turbine. Geotechnical data are obtained from studies available in the literature [8, 28]. The monopile design is performed according to the design guidelines by API and DNV-GL [3, 13]. The recently proposed p-y curves from the PISA project [8, 9], and t-z and Q-z springs from the unified method [19] are implemented for the analysis of the monopile design. The calculations are executed in Python, by importing the OpenSeesPy library as a non-linear solver [21, 29]. The monopile is modelled as a Timoshenko beam, considering p-δ effect. Once the monopile design is complete, the macroelements are first used to estimate the first natural frequency of the OWT, which as shown later in the manuscript is an important aspect in the design of the OWT system. Then predictions of the displacement are compared with results obtained from a finite element monotonic analysis. Analyses under cyclic loading are not within the scope of this work.

2 DESIGN OF THE MONOPILE FOUNDATION

This section presents a design scenario for a monopile foundation for a 8 MW offshore wind turbine located in 30 m water. The loads and the geotechnical conditions are selected from the literature and are applicable to monopiles installed in offshore homogeneous sand sites, under drained loading conditions. The monopile foundation is designed using the recent PISA methodology [8, 10]. This offers a more realistic approach to current large diameter monopiles with short embedment depth, compared to API formulations which were developed based on field tests of small diameter, flexible piles [7]. The design follows the API and DNV-GL guidelines summarized in Table 1. Working Stress Design (WSD) for the structural steel and soil bearing capacity checks and Serviceability Limit State (SLS) for the pile ground level displacement check are considered for the monopile design according to [3] and [13] guidelines, respectively.

Table 1: Monopile design checks according to API [3] and DNV-GL [13] guidelines

Guideline	**Checks**	**Condition**
API	Shear	$f_s = \frac{V}{0.5A} < F_s = 0.4F_y$
API	Combined	$\frac{f_a}{0.6F_{xc}} + \frac{\sqrt{f_{bx}^2+f_{by}^2}}{F_b} \leq 1.0$
API	Overload	$\frac{P/A}{F_{xc}} + \frac{2}{\pi}(\arcsin\frac{M/Z}{F_{xc}}) \leq 1.0$
API	Soil Bearing	$\frac{F_v}{A} \leq \frac{Q_c}{2} = \frac{Q_p+Q_{fc}}{2}$
DNV-GL	Service	$\delta < \frac{2L}{200}$

f_a is the absolute value of acting axial stress, f_{bx} is the absolute value of acting resultant bending stress in the x direction, f_{by} is the absolute value of acting resultant bending stress in y direction f_s is maximum beam shear stress, A is the cross-sectional area, F_b is allowable bending stress, F_s is allowable beam shear stress, F_{xc} is inelastic local buckling stress, F_y is yield strength, L is the total length of the monopile, M is the bending moment, P_v is axial loading, Q_c is the ultimate axial capacity of piles in compression, Q_{fc} is shaft friction capacity in compression, Q_p is the end bearing capacity V is transverse shear force, Z is the plastic modulus, δ is lateral displacement.

2.1 Geotechnical data and design loads

The site considered in this study includes a deep homogeneous soil layer of the Dunkirk sand [8, 28]. This way the rule-based PISA design approach can be adopted using pre-defined functions of the soil reaction curves, following the General Dunkirk sand model (GDSM), as described in the work of Burd *et al.* [8]. The foundation soil is a normally consolidated marine sand that originates from a coastal site in Northern France. The site includes a 3 m hydraulically placed sand at the top to increase the ground level in the 1970s without compaction or surcharging. In line with previous studies [8], this fill is not considered in the analysis, and a hydrostatic pore pressure distribution is assumed for the underlying sand. The CPT data along with selected design tip resistance values q_c (blue line) are given in Figure 1 ([28]). The relative density, D_R, is considered equal to 75%, and the critical state friction angle ϕ'_{cs} is 32°. All other geotechnical parameters necessary for the implementation of the PISA design approach, the macroelements and the rigorous three-dimensional finite element analysis are taken from relative publications of the PISA project [8, 28].

The OWT specifications and geometry, as well as pertinent design loads, are obtained from

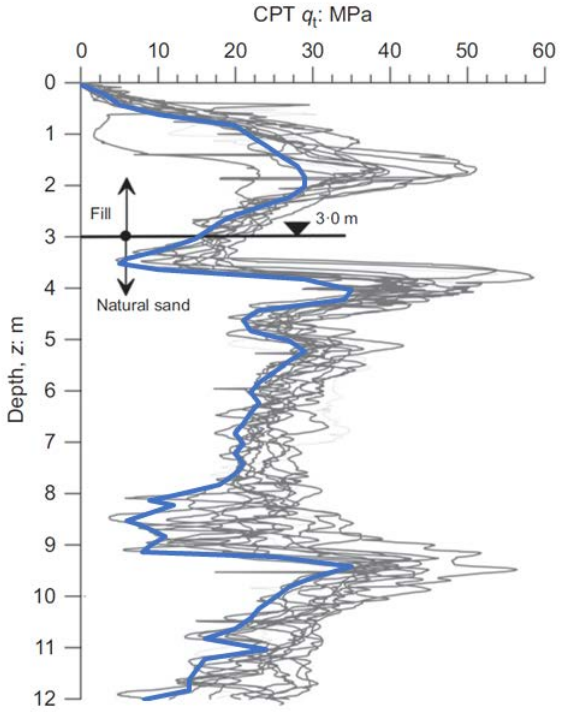

Figure 1: CPT data from sand soil profile in Dunkirk with selected design values (blue line) [28]

the work of Bhattacharya [7]. In particular, metocean data for the case of a 30 m water-deep site and 12 m of maximum wave height are used. The wind load depends on the wind speed, the rotor diameter, the controlling mechanism, and turbulence. The wave load depends on the water depth and the pile diameter. Typical lateral loads for the problem at hand are presented in Table 2. The vertical loads include the tower mass, m_T, together with rotor-nacelle assembly mass, m_{RNA}, and the dead weights of the monopile, m_P, and the transition piece, m_{TP}. Steel sections are made of $S355$ grade and unit weight of $78.6\ kN/m^3$. The following load cases are considered in the design [5, 7]: (1) normal operational conditions; (2) extreme wave load

Table 2: Typical wind and wave loads for an 8 MW offshore wind turbine according to Bhattacharya [7]

Input Parameter	**Symbol**	**Unit**	**Case Study**
Rotor diameter	D_{rotor}	m	164
Rated wind speed	U_r	m/s	13
Hub height	z_{hub}	m	110
Monopile diameter	D	m	7.5
Horizontal wind force	Fh_{wind}	MN	2.3
Horizontal wave force	Fh_{wave}	MN	6.1
Moment from wind force	M_{wind}	MN.m	323
Moment from waves	M_{wave}	MN.m	175
Tower mass	m_T	ton	558
Rotor-nacelle assembly mass (RNA)	m_{RNA}	ton	410

conditions; (3) extreme wind load conditions; (4) cut-out wind speed and extreme operating gust conditions; and (5) wind-wave misalignment condition (the same as in (2), only wind and wave act perpendicular).

2.2 p-y and t-z design analysis

The PISA method defines lateral load-displacement curves ($p - y$) and moment-rotation curves throughout the pile ($m - \theta$) and at the pile tip ($M_B - \theta$), as well as an additional base lateral load-displacement curve ($H_B - y$). The embedded pile is modelled as a Timoshenko beam, which allows for the realistic approximation of the shear strains in the pile [9]. An example of monopile discretization including lateral and axial springs is shown in Figure 2.

The PISA design method for sands is applicable to monopiles installed at offshore sand sites

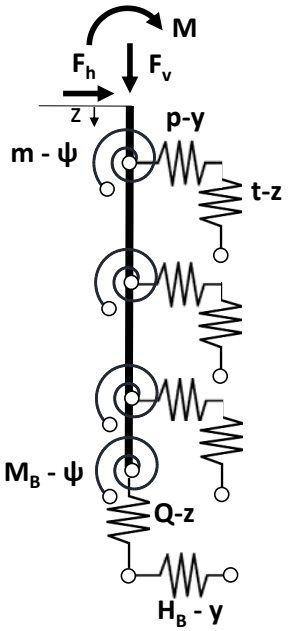

Figure 2: Pile discretization for the problem considered

with similar sand characteristics to the Flandrian sand found at Dunkirk, provided that the dimensions of the monopiles fall within the calibration space (i.e., $2 \leq L/D \leq 6, 5 \leq h/D \leq 15$, $45\% \leq D_R \leq 90\%$) [8]. In this work, only the load-displacement curves along the pile length i.e., $p-y$ curves, and an additional base lateral load-displacement curve $H_b - y$ are used.

The normalized soil reactions can be determined as a function of normalized displacements by the four-parameter conic function where the parameters are k the initial slope, $\bar{y_u}$ the ultimate normalized soil reaction, $\bar{x_u}$ the normalized displacement or rotation at the ultimate soil reaction, and k the shape parameter ($0 \leq n \leq 1$) of the soil reaction curve:

$$\bar{y} = \bar{y_u} \frac{2\,c}{-b + \sqrt{b^2 - 4ac}} \quad \text{for } \bar{x} \leq \bar{x_u} \quad \text{and} \quad \bar{y} = \bar{y_u} \quad \text{for } \bar{x} > \bar{x_u} \tag{1}$$

where

$$a = 1 - 2n, \qquad b = 2n\frac{\bar{x}}{\bar{x_u}} - (1-n)\left(1 + \frac{\bar{x}k}{\bar{y_u}}\right), \qquad c = \frac{\bar{x}k}{\bar{y_u}}(1-n) - n\frac{\bar{x}^2}{\bar{x_u}^2}$$

The actual values (p, y, m, θ, H_B, M_B) are determined from the normalized values ($\bar{p}$, $\bar{y}$, $\bar{m}$, $\bar{\theta}$, $\bar{H_B}$, $\bar{M_B}$).

For $p-y$ and $H_B - y$ curves:

$$\bar{p} = \frac{p}{\sigma'_{\text{vi}}\,D}, \quad \bar{H_B} = \frac{H_B}{\sigma'_{\text{vi}}\,D^2}, \quad \text{and} \quad \bar{y} = \frac{y\,G_0}{\sigma'_{\text{vi}}\,D}$$

For $m - \psi$ and $M_B - \psi$ curves:

$$\bar{m} = \frac{m}{|p|D} \quad \bar{M_B} = \frac{M_B}{\sigma'_{\text{vi}}\,D^3}, \quad \text{and,} \quad \bar{\psi} = \frac{\psi\,G_0}{\sigma'_{\text{vi}}} \tag{2}$$

where G_0 is the small-strain shear modulus defined according to [16]:

$$G_0 = \frac{B\,p'_{\text{ref}}}{0.3 + 0.7\,e_0^2}\sqrt{\frac{p'}{p'_{\text{ref}}}} \tag{3}$$

where p'_{ref} is 101.3 kPa, the atmospheric pressure.

The recently developed Unified Method is used for design under axial loads; comparisons against available methods demonstrated a very good performance in predicting the axial pile capacity [19]. This is a CPT-based method that is established using experimental data obtained from 71 static load tests of piles embedded in siliceous sand deposits. The plugging effect, effects of loading direction, sand-pile interface friction, friction fatigue, and radial stress changes during the loading of driven piles are considered. Axial deflection - axial force ($t-z$) curves and the tip deflection - axial force ($Q-z$) curve are presented in Figure 2.

Shaft capacity is calculated as follows:

$$Q_{\text{shaft}} = \pi D \int_0^L \tau_f\,dz \quad \text{where} \quad \tau_f = (f_t/f_c)(\sigma'_{\text{rc}} + \Delta\sigma'_{\text{rd}})\,\tan 29^\circ$$

$$\sigma'_{\text{rc}} = (q_c/44)\,A_{\text{re}}^{0.3}\,[\max(1,(L-z)/D)]^{-0.4} \quad \text{and} \quad \Delta\sigma'_{\text{rd}} = (q_c/10)\,(d_{\text{CPT}}/D)\left(\frac{q_c}{\sigma'_v}\right)^{-0.33}$$

$$A_{\mathrm{re}} = 1 - \mathrm{PLR}(D_i/D)^2 \quad \text{and} \quad \mathrm{PLR} \approx \tanh\left(0.3(D_i/d_{\mathrm{CPT}})^{0.5}\right)$$

where $f_t/f_c = 1$ in compression and 0.75 in tension. $d_{\mathrm{CPT}} = 35.7\mathrm{mm}$

Base capacity is calculated as follows:

$$Q_{\mathrm{base}} = q_{\mathrm{b0.1}}(\pi\, D^2/4) \quad \text{where} \quad q_{\mathrm{b0.1}} = (0.12 + 0.38\, A_{\mathrm{re}})q_p$$

$$q_p \approx q_{\mathrm{c,av,1.5D}} = \frac{1}{3D}\int_{L-1.5D}^{L+1.5D} q_c(z)\, dz$$

For the curves, z/z_{peak} vs. $t/t_{\max}$ and z/D vs. Q/Q_p tables from the API guideline [4] are held to define $t-z$ and $Q-z$ curves, respectively; where $t_{\max} = (\pi D\tau_f)$ and $Q_p = Q_{\mathrm{base}}$. As was recommended for routine design purposes, $z_{\mathrm{peak}} = 0.01\, D$ is considered [4].

The open-source software tool OpenSees is used for load-controlled analyses [21, 29]. Nonlinear algebraic equations are handled by Krylov Newton method. The analyses are carried out in ten load steps, each with an increment of 0.1, and the toleration level is set to 10^{-7} with a maximum iteration number of 1000. The hollow steel cylindrical monopile has an embedded length L_P, a free length L_S, a diameter D_P, a thickness t_P, a cross-sectional area A_P, a moment of inertia I_P, Young's modulus E_P, a plastic modulus Z_P, and a radius of gyration K_P. The monopile is modelled as a Timoshenko beam and the horizontal load and the moment transmitted from the OWT are applied at the mud level as a point load in OpenSees.

Final monopile design is shown in Figure 3. The minimum wall thickness is $t_P = 6.35 + D_P/100$ where D_P is in mm [3]. The embedded length is determined following a critical pile length methodology presented by Arany *et al.* [5]. According to this method, the pile length is obtained based on a critical length (beyond which an increment in the length has a negligible effect on the pile head displacement), which can be calculated based on pile diameter and relative pile-soil stiffness ratio.

3 SIMPLIFIED APPROACH USING MACRO ELEMENTS

The monopile-soil system can be represented by three impedances (macro elements) K_{LL}, K_{RR} and K_{LR} which correspond to swaying, rocking, and cross-swaying-rocking of the pile head, respectively. Figure 4 shows a simplified model of an OWT represented by a single degree of freedom system (SDOF) which rests on a "flexible base" represented by a set of macro elements. Prior to assessing the response of the OWT via the simplified approach, macroelements available in the literature are assessed on the basis of their ability to predict the natural frequency of the system.

3.1 Simple method to estimate the first natural frequency of an OWT

Calculating the first natural frequency of an offshore wind turbine-monopile system is crucial because it helps to ensure that the system can operate safely and efficiently. The natural frequency refers to the frequency at which a structure naturally vibrates when subjected to external forces or disturbances. In the case of an offshore wind turbine-monopile system, the natural frequency determines how the system will respond to wind and wave loads. If the natural frequency of the system is too low, it may experience resonance with the wind and wave

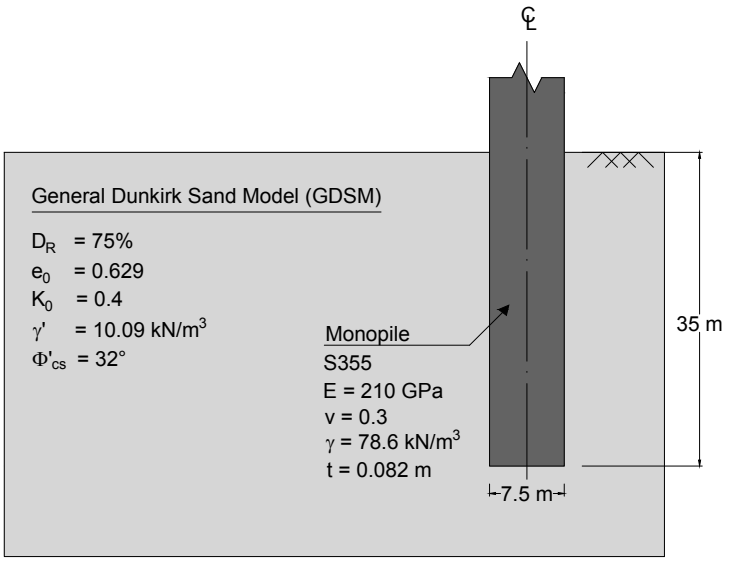

Figure 3: Final monopile design for an 8 MW OWT embedded in Dunkirk sand [8, 28].

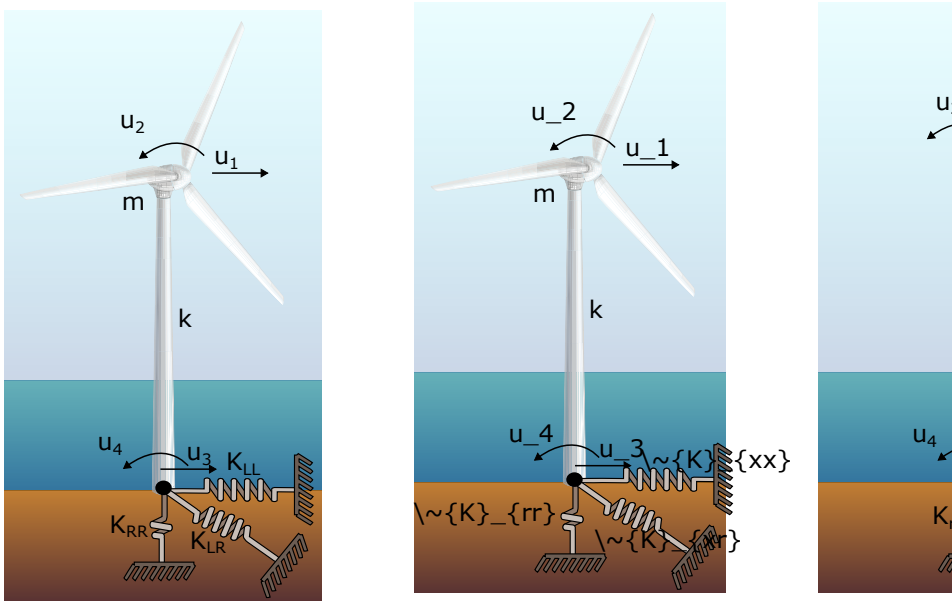

Figure 4: Schematic representation of an OWT which rests on a "flexible base".

loads, causing to excessive vibrations that can damage the structure and even cause it to fail. On the other hand, if the natural frequency is too high, the system may be too stiff and unable to absorb the dynamic loads from wind and waves, again leading to damage and failure. By calculating the first natural frequency of the offshore wind turbine-monopile system, engineers can determine whether the system's design and construction are adequate to withstand the environmental loads and operate safely and efficiently. Arany *et al.* [6] show typical wind and wave spectra, rotational speed (1P) and blade passing (3P) frequency bands for six commercial turbines as was given in Figure 5. The first natural frequency f_1 is intended to lie within the gap

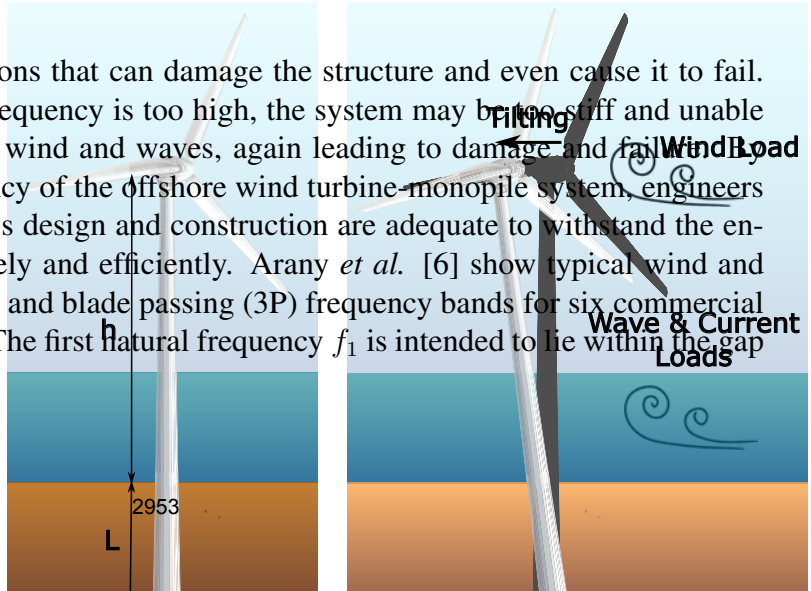

between 1P and 3P. Otherwise, adjustments can be made to the system's design or operation to ensure that it can function as intended.

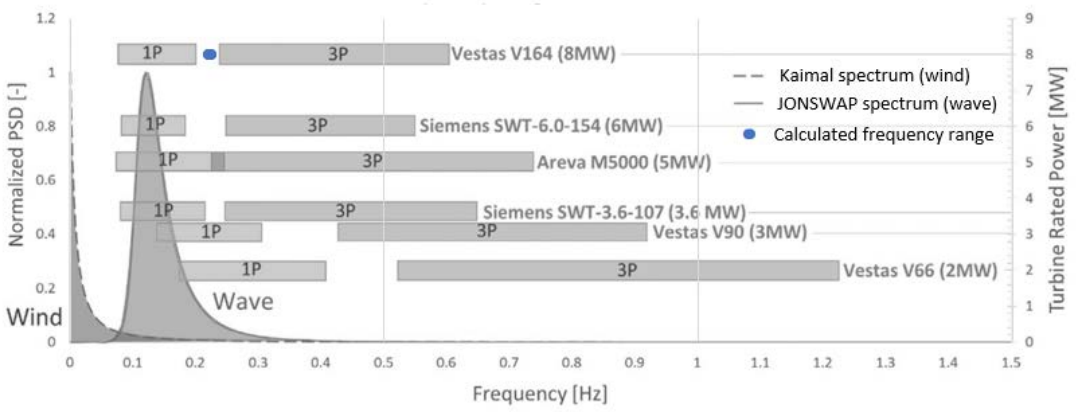

Figure 5: Typical wind and wave spetra together with 1P and 3P frequency bands for six commercial turbines (modified from [6])

In this work, the simplified methodology proposed by Arany *et al.* is used to obtain the first natural frequency of the OWT-monopile system using data from the Wind Turbine Generator, the tower and monopile geometry, and the foundation soil properties [5]. These data are included in Table 3. The tower refers to an 8MW offshore wind turbine as described in [12]. The

Table 3: Input parameters to estimate f_1

Input Parameter	**Symbol**	**Unit**	**Case Study**
Tower height	L_T	m	106.3
Tower bottom diameter	D_t	m	7.7
Tower top diameter	D_b	m	5
Average tower wall thickness	t_T	m	0.029
Tower Young's modulus	E_T	GPa	210
Platform height above mudline	L_S	m	45
Monopile diameter	D_P	m	7.5
Monopile embedment length	L_P	m	35
Monopile wall thickness	t_P	m	0.082
Monopile Young's modulus	E_P	GPa	210
Monopile Poisson's ratio	ν	-	0.3

expressions were derived by modelling the rotor– nacelle assembly (RNA) as a lumped top head mass, m_{RNA}, and the tower and the substructure as beams. The tower diameter is assumed to linearly decrease from D_b at the bottom to D_t at the top of the tower. The average diameter is used as the equivalent constant diameter for the idealised tower, D_T. The wall thickness t_T is also assumed to be constant along the tower. The soil-foundation interaction is modelled by three springs characterised by lateral K_{LL}, rotational K_{RR}, and cross coupling K_{LR} stiffness, respectively.

The first natural frequency f_1 is obtained by multiplying the fixed base natural frequency f_{FB} by two factors, namely C_R and C_L, which take into account the flexibility of the foundation:

$$f_1 = C_R\, C_L\, f_{FB} \tag{4}$$

where

$$f_{FB} = \sqrt{\frac{1}{1+(1+\psi)^3\chi-\chi}}\, f_{FB,T} \qquad \chi = \frac{E_T\, I_T}{E_P\, I_P} \qquad \psi = \frac{L_S}{L_T}$$

χ is the bending stiffness ratio and ψ is the platform-to-tower length ratio. $E_T\, I_T$ is the bending stiffness of the tower, $E_P\, E_p$ is the bending stiffness of the monopile, L_S is the platform height above the seabed (represented by the distance from the mud line to the top of the transition piece), and L_T is the height of the tower. $f_{FB,T}$ is the fixed base natural frequency of the tower:

$$f_{FB,T} = \frac{1}{2\pi}\sqrt{\frac{3\, E_T\, I_T}{L^3\left(m_{RNA}+\frac{33}{140}m'_T\right)}} \tag{5}$$

In the previous equation m'_T is the mass of the tower and m_{RNA} is the mass of the rotor–nacelle assembly. The second moment of area, I_T, and the mass, m'_T, are calculated considering an average diameter D_T and an average wall thickness t_T:

$$I_T = \frac{1}{8}\,\pi\, D_T^3\, t_T \qquad m'_T = \rho_T\, D_T\, \pi\, t_T\, L_T \tag{6}$$

In Equation (4) C_R and C_L are empirical foundation flexibility factors:

$$C_R = 1\, -\, \frac{1}{1+a\left(\eta_R-\frac{\eta_{LR}^2}{\eta_L}\right)} \qquad C_L = 1\, -\, \frac{1}{1+b\left(\eta_L-\frac{\eta_{LR}^2}{\eta_R}\right)} \tag{7}$$

where $a = 0.6$ and $b = 0.5$ are empirical constants obtained as described in [5]. η_L, η_{LR} and η_R are the non-dimensional lateral, cross-coupling and rotational stiffness values, respectively:

$$\eta_L = \frac{K_{LL}\, L_T^3}{EI_\eta} \qquad \eta_{LR} = \frac{K_{LR}\, L_T^2}{EI_\eta} \qquad \eta_R = \frac{K_{RR}\, L_T}{EI_\eta} \tag{8}$$

EI_η represents the equivalent bending stiffness of the tapered tower:

$$EI_\eta = E_T\, I_t\left(\frac{1}{3}\,\frac{2q^2\,(q-1)^3}{2q^2\,\ln q - 3q^2 + 4q - 1}\right) \tag{9}$$

where I_t is the second moment of area at the top of the tower, and $q = D_b/D_t$. The applicability of Equation 7 is limited to:

$$\eta_R > 1.2\frac{\eta_{LR}^2}{\eta_L} \qquad \eta_L > 1.2\frac{\eta_{LR}^2}{\eta_R} \tag{10}$$

Available macro elements The pile head stiffness or macro elements can be estimated by analytical formulations available in literature, as suggested by [5]. The appropriate method for the pile head stiffness estimation depends on the pile behavior (i.e., rigid or slender). Piles can be considered rigid if the pile moves as a whole and does not deflect under operational loads [7]. This study considers both slender and rigid pile macroelement derivations to obtain K_{LL}, K_{LR} and K_{RR}:

i. Macro-elements derived for slender piles

Parabolic inhomogeneous soils $n = 0.5$

Gazetas (1984) [14]:

$$K_{\mathrm{LL}} = 0.79 E_{S0} D_P \left(\frac{E_{eq}}{E_{S0}}\right)^{0.28} \quad K_{\mathrm{LR}} = -0.24 E_{S0} D_P^2 \left(\frac{E_{eq}}{E_{S0}}\right)^{0.53} \quad K_{\mathrm{RR}} = 0.15 E_{S0} D_P^3 \left(\frac{E_{eq}}{E_{S0}}\right)^{0.77}$$

Pender(1993) [23]:

$$K_{\mathrm{LL}} = 0.735 E_{S0} D_P \left(\frac{E_{eq}}{E_{S0}}\right)^{0.33} \quad K_{\mathrm{LR}} = -0.27 E_{S0} D_P^2 \left(\frac{E_{eq}}{E_{S0}}\right)^{0.55} \quad K_{\mathrm{RR}} = 0.1725 E_{S0} D_P^3 \left(\frac{E_{eq}}{E_{S0}}\right)^{0.776}$$

Shadlou and Bhattacharya (2016) [26]:

$$K_{\mathrm{LL}} = \frac{1.02 E_{S0} D_P}{f_{(V_s)}} \left(\frac{E_{eq}}{E_{S0}}\right)^{0.27} \quad K_{\mathrm{LR}} = \frac{-0.29 E_{S0} D_P^2}{f_{(V_s)}} \left(\frac{E_{eq}}{E_{S0}}\right)^{0.52} \quad K_{\mathrm{RR}} = \frac{0.17 E_{S0} D_P^3}{f_{(V_s)}} \left(\frac{E_{eq}}{E_{S0}}\right)^{0.76}$$

ii. Macro-elements derived for rigid piles

Homogeneous soils $n = 0$

Poulos and Davis (1980) [24]:

$$K_{\mathrm{LL}} = k_h D_p L_p \qquad K_{\mathrm{LR}} = \frac{-k_h D_p L_p^2}{2} \qquad K_{\mathrm{RR}} = \frac{k_h D_p L_p^3}{3}$$

Shadlou and Bhattacharya (2016) [26]:

$$K_{\mathrm{LL}} = \frac{3.2 E_{S0} D_P}{f_{(V_s)}} \left(\frac{L_P}{D_P}\right)^{0.62} \quad K_{\mathrm{LR}} = \frac{-1.7 E_{S0} D_P^2}{f_{(V_s)}} \left(\frac{L_P}{D_P}\right)^{1.56} \quad K_{\mathrm{RR}} = \frac{1.65 E_{S0} D_P^3}{f_{(V_s)}} \left(\frac{L_P}{D_P}\right)^{2.5}$$

Linear inhomogeneous soils $n = 1$

Poulos and Davis (1980) [24]:

$$K_{\mathrm{LL}} = \frac{1}{2} L_p^2 n_h \qquad K_{\mathrm{LR}} = -\frac{1}{3} L_p^3 n_h \qquad K_{\mathrm{RR}} = \frac{1}{4} L_p^4 n_h$$

Shadlou and Bhattacharya (2016) [26]:

$$K_{\mathrm{LL}} = \frac{2.35 E_{S0} D_P}{f_{(V_s)}} \left(\frac{L_P}{D_P}\right)^{1.53} \quad K_{\mathrm{LR}} = \frac{-1.775 E_{S0} D_P^2}{f_{(V_s)}} \left(\frac{L_P}{D_P}\right)^{2.5} \quad K_{\mathrm{RR}} = \frac{1.58 E_{S0} D_P^3}{f_{(V_s)}} \left(\frac{L_P}{D_P}\right)^{3.45}$$

Parabolic inhomogeneous soils $n = 0.5$

Shadlou and Bhattacharya (2016) [26]:

$$K_{\mathrm{LL}} = \frac{2.66 E_{S0} D_P}{f_{(V_s)}} \left(\frac{L_P}{D_P}\right)^{1.07} \quad K_{\mathrm{LR}} = \frac{-1.8 E_{S0} D_P^2}{f_{(V_s)}} \left(\frac{L_P}{D_P}\right)^{2.0} \quad K_{\mathrm{RR}} = \frac{1.63 E_{S0} D_P^3}{f_{(V_s)}} \left(\frac{L_P}{D_P}\right)^{3.0}$$

Table 4: Stiffness coefficients for the reference soil-foundation system according to existing rigid pile formulations and related natural frequency

	Homogeneous $n = 0$		Linear inhomogeneous $n = 1$		Parabolic inhomogeneous $n = 0.5$
	[24]	[26]	[24]	[26]	[26]
K_{LL}	10.50	10.39	24.50	21.94	26.41
K_{LR}	-183.75	-176.12	-571.67	-553.79	-561.59
K_{RR}	4287.50	5454.64	15006.25	15974.32	17799.31
f_1	0.221	0.223	0.222	0.223	0.224

where

$$E_{eq} = \frac{E_p I_p}{D_p^4 \pi / 64}, \qquad f_{(v_s)} = 1 + |v_s - 0.25| \tag{11}$$

k_h is the modulus of subgrade reaction, n_h is the coefficient of subgrade reaction (the rate of increase of k_h with depth) where $k_h = n_h(z/D_P)$ for sand [7].

E_{S0} is the soil stiffness at $z = -D_P$. In Dunkirk site, the G_0 as was given in Equation 3 together with $E = G_0(2(1 + \mu))$ expression is held. A linear profile is fit considering the parabolic inhomogeneous soil stiffness (see Figure 6). Homogeneous soil stiffness is calculated following $[E_P/E_{S0}]_{linear} = 0.24\,[E_P/E_S]^{1.25}_{homogeneous}$ [27] to keep the lateral response in homogeneous and linear soil profiles equal. Calculated parabolic soil stiffness profile- and adopted homogeneous and linear soil stiffness profiles are shown in Figure 6.

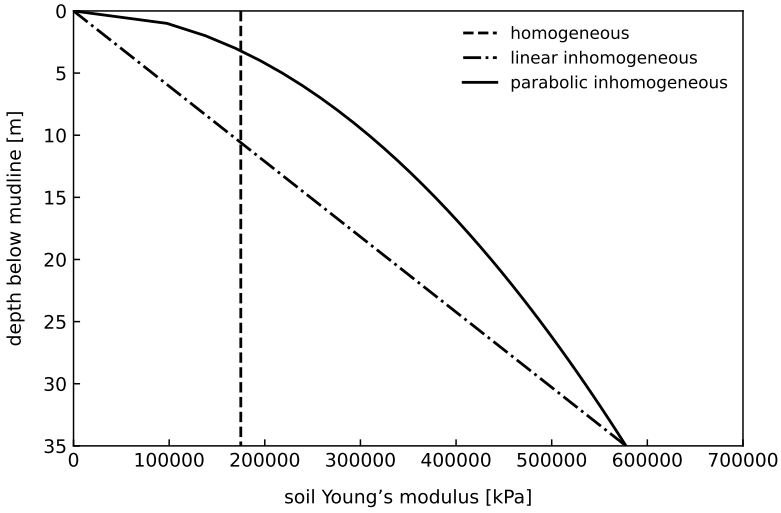

Figure 6: Homogeneous, linear, and parabolic soil stiffness profiles

The stiffness coefficients values adopted for the natural frequency estimation for rigid piles are reported in Table 4 for rigid pile estimation and Table 5 by slender pile estimation. K_{LL} in GN/m, K_{LR} in GN, and K_{RR} in GNm/rad. The natural frequency values for the presented structure-substructure-foundation system, estimated by the described methodology, are reported in the same table in Hz.

Table 5: Stiffness coefficients for the reference soil-foundation system according to existing slender pile formulations and related natural frequency

	Parabolic inhomogeneous $n = 0.5$		
	[14]	[23]	[26]
K_{LL}	5.13	5.89	6.05
K_{LR}	-33.38	-40.84	-36.84
K_{RR}	428.42	505.25	443.42
f_1	0.211	0.212	0.212

For the OWT at hand, the rotational frequency range (1P) is $0.105 - 0.175\,Hz$ and the turbine's blade passing frequency range (3P) is $0.315 - 0.525\,Hz$, as derived by the rotor speeds information provided by [6]. For the widely used soft–stiff design, the target first natural frequency must lie in the range between the maximum of 1P (0.175 Hz) and the minimum of 3P (0.315 Hz). The results reported in Table 4 and 5 show that the formulation for the stiffness coefficients does not affect the frequency estimation and that, according to the applied computation methodology, the design requirement is satisfied.

3.2 Displacement and rotation at sea bed level

Following Figure 4, the displacement and rotation of the monopile at the the level of the sea bed, u_3 and u_4, respectively, can be determined by the following matrix form equation:

$$\begin{bmatrix} F \\ M \end{bmatrix} = \begin{bmatrix} K_{LL} & K_{LR} \\ K_{LR} & K_{RR} \end{bmatrix} \cdot \begin{bmatrix} u_3 \\ u_4 \end{bmatrix} \tag{12}$$

The response of the offshore wind turbine is defined by the lateral displacement, u_1, and tilt or rotation, u_2. The response at the top is linked to the response at the seabed level by the turbine mass, m, and the tower stiffness, k.

The mud-line pile displacements for the presented structure-substructure-foundation system, estimated by different methods, are shown in Figure 7. Such displacements are calculated by the soil small-strain stiffness where the system is not expected to go into the nonlinear regime under free vibrations. However, the soil behavior is expected to be nonlinear under such high loads applied to the monopile.

Macroelements obtained for a homogeneous soil profile are deemed to be the most accurate representation of an elastic and homogeneous soil profile under lateral loading within the designated range of design loads. On the other hand, macroelements derived for a parabolic soil profile are considered to be the least precise representation of such a soil profile under lateral loading within the same range of design loads. This discrepancy can be attributed to the linear soil stiffness profile fit illustrated in Figure 6. Additional analyses are required to seek the more accurate macroelements for a parabolic inhomogeneous soil profile at hand.

4 3D FINITE ELEMENT MODEL

In order to predict the nonlinear load-deformation response, 3D FE analysis is held via OpenSees [21, 29]. Gmsh [15] is used for the mesh discretization, and gmsh2opensees module [1] is held to extract nodes and elements from gmsh to OpenSees. The axisymmetric finite element model has a computational domain size $L_x = 100\mathrm{m}, L_y = 50\mathrm{m}, L_z = 50\mathrm{m}$ as presented in Figure 8. The soil surrounding the pile, the plugged soil inside the pile, and the pile itself are modelled with standard four-node tetrahedron elements with one Gauss integration

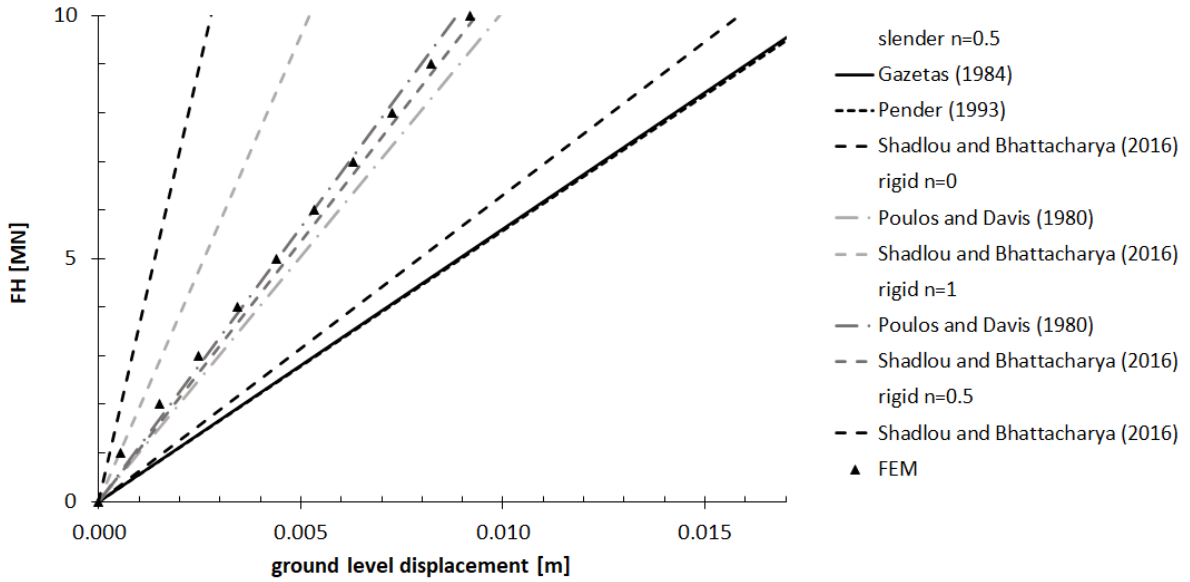

Figure 7: Pile lateral displacement at the mud-line

point (FourNodeTetrahedron elements in OpenSeesPy library). The boundary conditions for the model are a fixed bottom surface, a free upper surface, and no horizontal displacement perpendicular to the lateral surfaces. Axisymmetry surfaces are fixed in y direction 8.

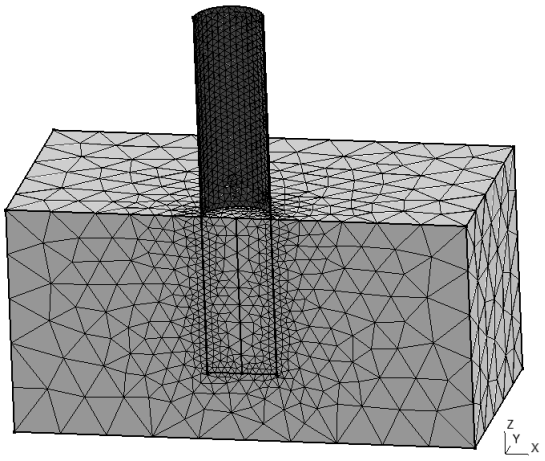

Figure 8: 3D FE model

The material of monopile is elastic (ElasticIsotropic in OpenSeesPy library) with material properties given in Table 3 for embedded and free lengths of 35 and $45\mathrm{m}$ respectively. The lateral force is applied at the top of the model with an eccentricity, h, of $45\mathrm{m}$ in this case. This eccentricity value, $h = L_s$, is consistent with the relevant small-scale testing studies where $h \approx 1.2L_P$ [18, 20]. The material for soil is assumed elastic (ElasticIsotropic in OpenSeesPy library) with the homogeneous profile with Young's modulus given in Table 6. Initial K_0 analysis before pile installation is followed by wished-in-place pile condition analysis. Then, the load is applied

in 10 steps in a load-controlled way. The convergence is sought with a relative normal increment within a tolerance of 0.001 similar to [20]. Displacement results are shown in Figure 9 for a maximum load of 10 MN. Displacements are visually scaled 10 times for better representation.

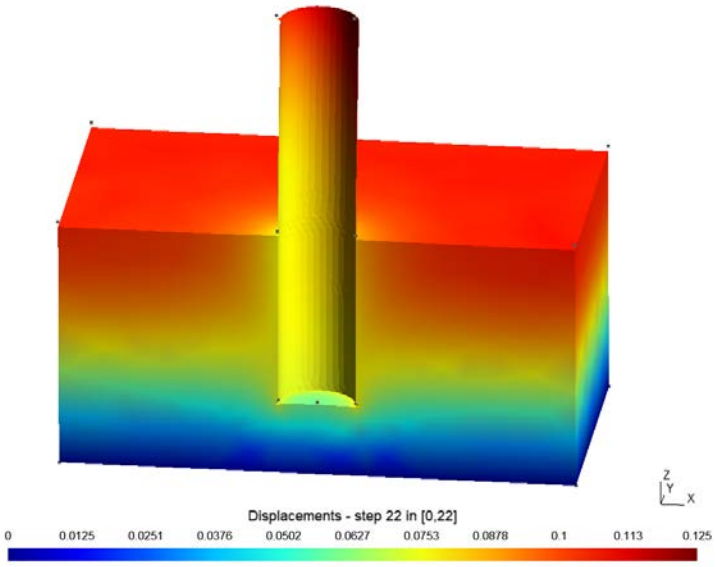

Figure 9: 3D FEA model displacement field [m]

5 CONCLUSIONS

This study aims to test a simplified method for predicting the displacement and rotation of OWTs by using readily available macroelements to represent the monopile-foundation system. The main findings of this study can be summarized as follows:

- Although the stiffness coefficients of macroelements diverge for different soil profile configurations (homogeneous, linear inhomogeneous, and parabolic inhomogeneous), they converge to a similar natural frequency (see Figure 5).
- The influence of the macroelement stiffness coefficients on frequency estimation is negligible and between the design limits for the 8 MW OWT designed.
- Macroelements derived for homogeneous soil profile are the most accurate representation of an elastic, homogeneous soil profile under lateral loading within the designated range of design loads.
- Macroelements derived for parabolic soil profile are the least accurate representation of an elastic, homogeneous soil profile under lateral loading within the designated range of design loads. This can be associated with the linear soil stiffness profile shown in Figure 6.

Acknowledgements

The research proposed in this paper was supported by the *Cyclic soil-structure interaction framework for the foundations of offshore renewable energy structures* project, funded by the "KU Leuven Global PhD Partnerships with The University of Melbourne" scheme (GPUM/21/023).

References

[1] J. A. Abell. *gmsh2opensees*, 2022. A simple Python module to use Gmsh and OpenSees together in Python.

[2] E. An. Strategy to harness the potential of offshore renewable energy for a climate neutral future. *European Commission: Brussels, Belgium*, 2020.

[3] API. *RP2A-WSD: Recommended Practice for Planning, Designing and Constructing Fixed Offshore Platforms – Working Stress Design*. American Petroleum Institute, 2014.

[4] API. *RP2GEO: Geotechnical and Foundation Design Considerations*. American Petroleum Institute, 2014.

[5] L. Arany, S. Bhattacharya, J. Macdonald, and S. Hogan. Design of monopiles for offshore wind turbines in 10 steps. *Soil Dynamics and Earthquake Engineering*, 92:126–152, 2017.

[6] L. Arany, S. Bhattacharya, J. H. Macdonald, and S. J. Hogan. Closed form solution of eigen frequency of monopile supported offshore wind turbines in deeper waters incorporating stiffness of substructure and ssi. *Soil Dynamics and Earthquake Engineering*, 83:18–32, 2016.

[7] S. Bhattacharya. *Design of foundations for offshore wind turbines*. John Wiley & Sons, 2019.

[8] H. J. Burd, D. M. Taborda, L. Zdravković, C. N. Abadie, B. W. Byrne, G. T. Houlsby, K. G. Gavin, D. J. Igoe, R. J. Jardine, C. M. Martin, et al. Pisa design model for monopiles for offshore wind turbines: application to a marine sand. *Géotechnique*, 70(11):1048–1066, 2020.

[9] B. W. Byrne, G. T. Houlsby, H. J. Burd, K. G. Gavin, D. J. Igoe, R. J. Jardine, C. M. Martin, R. A. McAdam, D. M. Potts, D. M. Taborda, et al. Pisa design model for monopiles for offshore wind turbines: application to a stiff glacial clay till. *Géotechnique*, 70(11):1030–1047, 2020.

[10] B. W. Byrne, R. A. McAdam, H. J. Burd, W. J. Beuckelaers, K. G. Gavin, G. T. Houlsby, D. J. Igoe, R. J. Jardine, C. M. Martin, A. Muir Wood, et al. Monotonic laterally loaded pile testing in a stiff glacial clay till at cowden. *Géotechnique*, 70(11):970–985, 2020.

[11] G. W. E. Council. Global offshore wind report 2022. *Global Wind Energy Council: Brussels, Belgium*, 2022.

[12] C. Desmond, J. Murphy, L. Blonk, and W. Haans. Description of an 8 mw reference wind turbine. *Journal of Physics: Conference Series*, 753:092013, 09 2016.

[13] DNV-GL. Support structures for wind turbines. *Offshore Standard DNVGL-ST-126*, 2016.

[14] G. Gazetas. Seismic response of end-bearing single piles. *International Journal of Soil Dynamics and Earthquake Engineering*, 3(2):82–93, 1984.

[15] C. Geuzaine and J.-F. Remacle. Gmsh: A 3-d finite element mesh generator with built-in pre-and post-processing facilities. *International journal for numerical methods in engineering*, 79(11):1309–1331, 2009.

[16] B. O. Hardin and W. L. Black. Vibration modulus of normally consolidated clay. *Journal of the Soil Mechanics and Foundations Division*, 94(2):353–369, 1968.

[17] G. Houlsby, C. Abadie, W. Beuckelaers, and B. Byrne. A model for nonlinear hysteretic and ratcheting behaviour. *International Journal of Solids and Structures*, 120:67–80, 2017.

[18] C. LeBlanc, G. Houlsby, and B. Byrne. Response of stiff piles in sand to long-term cyclic lateral loading. *Géotechnique*, 60(2):79–90, 2010.

[19] B. Lehane, Z. Liu, E. Bittar, F. Nadim, S. Lacasse, R. Jardine, P. Carotenuto, P. Jeanjean, M. Rattley, K. Gavin, et al. A new'unified'cpt-based axial pile capacity design method for driven piles in sand. In *4th International Symposium on Frontiers in Offshore Geotechnics*, pages 463–477. American Society of Civil Engineers, 2020.

[20] H. Liu, E. Kementzetzidis, J. A. Abell, and F. Pisanò. From cyclic sand ratcheting to tilt accumulation of offshore monopiles: 3d fe modelling using sanisand-ms. *Géotechnique*, 72(9):753–768, 2022.

[21] S. Mazzoni, F. McKenna, M. H. Scott, G. L. Fenves, et al. *OpenSees command language manual*, volume 264. Berkeley, California, United States, 2006.

[22] O. Orakci, N. Huvaj, S. François, and G. Anoyatis. Probability of unsatisfactory performance of monopile foundations for offshore wind turbines considering variations in seabed properties. *Ocean Engineering*, 277:114335, 2023.

[23] M. J. Pender. Aseismic pile foundation design analysis. *Bulletin of the New Zealand National Society for Earthquake Engineering*, 26:49–160, 1993.

[24] H. G. Poulos, E. H. Davis, et al. *Pile foundation analysis and design*, volume 397. Wiley New York, 1980.

[25] L. Ramirez, D. Fraile, and G. Brindley. Offshore wind in europe: Key trends and statistics 2020. 2021.

[26] M. Shadlou and S. Bhattacharya. Dynamic stiffness of monopiles supporting offshore wind turbine generators. *Soil Dynamics and Earthquake Engineering*, 88:15–32, 2016.

[27] K. C. Syngros. *Seismic response of piles and pile-supported bridge piers evaluated through case histories*. City University of New York, 2004.

[28] L. Zdravković, R. J. Jardine, D. M. Taborda, D. Abadias, H. J. Burd, B. W. Byrne, K. G. Gavin, G. T. Houlsby, D. J. Igoe, T. Liu, et al. Ground characterisation for pisa pile testing and analysis. *Géotechnique*, 70(11):945–960, 2020.

[29] M. Zhu. The openseespy library. `https://openseespydoc.readthedocs.io/en/latest/index.html#`, 2019. Accessed: 2021-11-20.